

FAULT PLANE SOLUTIONS AND RELOCATIONS OF RECENT
EARTHQUAKES IN MIDDLETON PLACE SUMMERVILLE
SEISMIC ZONE NEAR CHARLESTON, SOUTH CAROLINA

BY SRIRAM MADABHUSHI AND PRADEEP TALWANI

ABSTRACT

The Middleton Place Summerville Seismic Zone (MPSSZ), located about 20 km northwest of Charleston is the most active seismic zone in South Carolina. Between 1980 and 1991, 58 events with M_d 0.8 to 3.3 were recorded in MPSSZ. They lie in a diffuse area of 11 km by 14 km of which over two-thirds are located in a narrow 5 km by 6-km zone. The hypocentral depths range from 2 to 11 km with over 90% deeper than 4 km.

Single fault plane solutions were obtained for 35 events. Based on the focal mechanisms the earthquakes were grouped into five subsets. The mean P -axis of all fault plane solutions is oriented $N63^\circ E$, in general agreement with the direction of S_{Hmax} obtained from *in situ* stress measurements.

Of the 35 events, 18 are associated with reverse faulting on NW-SE striking and SW dipping fault planes. These events were inferred to be associated with the Ashley River fault zone, which is not a planar feature, but is composed of short segments of varying strikes ($N20^\circ W$ to $N70^\circ W$) and dips (40° to $70^\circ SW$). Eleven events were associated with strike-slip motion on NNE-SSW striking vertical faults and with thrust faulting on N-S oriented faults dipping to the west, respectively. These two sets are identified as being parts of the Woodstock fault zone.

The concentrated zone of seismicity included events associated with both the ARF and WF zones suggesting that it is at the intersection of these two fault zones.

INTRODUCTION

In a search for the structural control of the seismicity near Charleston, South Carolina, geophysical and geological data were acquired from the late 1970s to early 1980s (Rankin, 1977; Gohn, 1983). These complemented the seismicity data acquired from a local network since 1974. Reviews of studies (Talwani, 1985) and hypotheses (Dewey, 1985 and White and Long, 1989) put forward to explain the seismicity near Charleston, point to a lack of a consensus in our understanding of the cause and nature of seismicity.

In the eastern U.S., where surficial evidence for seismogenic faults is sparse, the nature of such features has to be determined indirectly. One method applicable in the Charleston region is to determine the hypocenters of microearthquakes and to obtain their fault plane solutions. In this paper we report on the analyses of instrumentally recorded seismicity in the Charleston area between 1980 and 1991.

SEISMOLOGICAL BACKGROUND

The nature of instrumentally recorded seismicity near Charleston was the subject of papers by Tarr (1977); Tarr *et al.*, (1981); Talwani (1982); Tarr and Rhea (1983); Talwani (1986); Rhea (1987) and Shedlock (1987, 1988). The results of these studies were summarized in Bollinger *et al.*, (1991). An early

result of these studies was the identification of a clustered pattern of seismicity in the South Carolina Coastal Plain (Tarr *et al.*, 1981). These studies identified three distinct zones of seismicity—(1) the Middleton Place Summerville Seismic Zone (MPSSZ), (2) the Adams Run Seismic Zone (ARSZ), located about 30 km southwest of MPSSZ, and (3) the Bowman Seismic Zone (BSZ) located about 60 km northwest of MPSSZ. Located about 20 km northwest of Charleston and coincident with the meizoseismal area of the 1886 Charleston earthquake, the MPSSZ is the most active seismic zone in South Carolina (Fig. 1a).

Talwani (1982), using a 2D seven-layer velocity model relocated the instrumentally recorded earthquakes in the MPSSZ. He identified two faults from the alignment of relocated hypocenters. A shallow, northwest-trending fault, defined by hypocenters 4 to 8 km deep striking parallel to the Ashley River, was labeled Ashley River fault (ARF). It overlies the deeper north-northeasterly trending Woodstock fault (WF) defined by planar distribution of hypocenters of focal depths between 9 and 13 km. Conversely, Rhea (1987) using a velocity gradient model, did not observe any planar alignment and interpreted the MPSSZ as a north-south trending diffuse zone of hypocenters about 28 km long and 14 km wide. Hypocentral depths calculated by Rhea were between about 2 and 10 km.

Composite focal mechanism solutions of the events supporting the northwest striking ARF by Tarr *et al.*, (1981) and Talwani (1982) and a single event focal mechanism for the magnitude 3.8 event on 22 November 1974 (Tarr, 1977) indicated that the seismicity was occurring on a steep southwesterly dipping fault by reverse faulting, with the southwest side upthrown. Composite fault plane solutions (CFPS) of other events suggested that the WF was associated with right lateral strike slip motion (Talwani, 1982). A common feature of the focal mechanism solutions was that the *P*-axes are subhorizontal and oriented ENE-WSW, consistent with other stress estimates in the region (e.g., Zoback *et al.*, 1987).

Shedlock (1987, 1988) relocated all the instrumentally recorded earthquakes between 1974 and 1986 in the South Carolina Coastal Plain. The events were located using a 3D velocity model (Shedlock and Roecker, 1987) and both *P*- and *S*-wave phase data. Of the 74 events that Shedlock relocated, over 50 (~68%) were located in the MPSSZ. These events defined a broad north-south zone about 22 km long and 12 km wide, with hypocentral depths between near surface to about 12 km, systematically deeper in the western part and shallower in the the eastern part of the MPSSZ. Shedlock obtained single event fault plane solutions (SFPS) for many of the located events. The number of stations used to obtain focal mechanisms varied greatly—from as few as four up to 17 in some cases. In the 1988 study, Shedlock obtained 20 single event fault plane solutions which described thrust, strike-slip, and normal faulting on planes showing no preferred orientation or dip. Based on their low magnitudes, spatial distribution, variety in the style of faulting, and orientation and dip of fault planes, Shedlock concluded that the seismicity was similar to the aftershock regions of other intraplate earthquakes and represented readjustment of the stress field over the affected volume. The inferred orientation of the maximum horizontal stress was NE-SW, consistent with earlier results.

THIS STUDY

In an effort to determine the tectonic association of the seismicity recorded in the MPSSZ, we examined 58 events occurring between September, 1980 and

November, 1991, in an area of about 300 km² lying between 32°52' to 33°03'N and 80°05' to 80°16'W. The well-recorded data in this period were chosen to complement the earlier study (Talwani, 1982), incorporating the events that occurred between 1974 and 1980. For locating the earthquakes we used published *P*-arrival times for events between 1980 and 1986 (Shedlock, 1987). By carefully going through the seismograms and the polarity information that were available at the United States Geological Survey facilities in Denver, all the first arrivals for each event were independently checked (by P.T.). This resulted in a few changes for the data between 1980 and 1986. For the earthquakes recorded after 1986, we have phase data available at the University of South Carolina on analog tape play backs. In all cases unambiguous picks were used. Using these data, events were relocated using the *P*-wave velocity model by Stihler (1985), (Table 1). We used *P*-wave polarities almost exclusively because the V_p/V_s ratio varies greatly with depth (Rhea, 1989) and the *S*-wave velocity model is not as well determined as Stihler's (1985) *P*-wave velocity model. Also reliable *S*-wave data were not available for most events and in order to obtain a homogenous data set, only *P*-wave arrivals were used.

Most of the epicenters lie in a 11 km by 14 km area between Middleton Place (MP) and Summerville (Fig. 1a) with an apparent concentration to the northwest of MP (Figure 1b) with no obvious spatial pattern of seismicity. The epicenters shown in Figure 1a include locations of all qualities. Of the 58 events located using HYPO71 ((Table 2), Lee and Lahr, 1975) 12, 29, 15, and 2, respectively, were of A, B, C, and D qualities.

The uniqueness and the stability of the solutions were tested in a manner similar to that described by Johnston *et al.* (1985). The solutions were found to be unique and stable and the depths are considered to be reliable. The locations obtained in this study were compared with those by Shedlock, (1987) for the events up to 1986 and with those in SEUSSN reports after 1986. For the relocated events, there were small changes (< 500 m) in the epicentral locations, and the focal depths obtained vary on an average by ± 1 km. Figure 1c shows cross sectional locations of the events along N-S and W-E lines (AA' and BB'). The events are located between depths of 1.9 km and 10.5 km but do not delineate any obvious fault planes. The spatial distribution is discussed later.

TABLE 1
VELOCITY MODEL USED IN THE RELOCATION
OF MPSSZ EARTHQUAKES

Depth to the Top of the Layer (km)	Velocity (km/sec)
00.00	2.20
00.75	5.50
01.50	5.60
03.00	5.75
07.00	5.90
10.00	6.45
20.00	6.70
32.60	8.12

(Stihler, 1985)

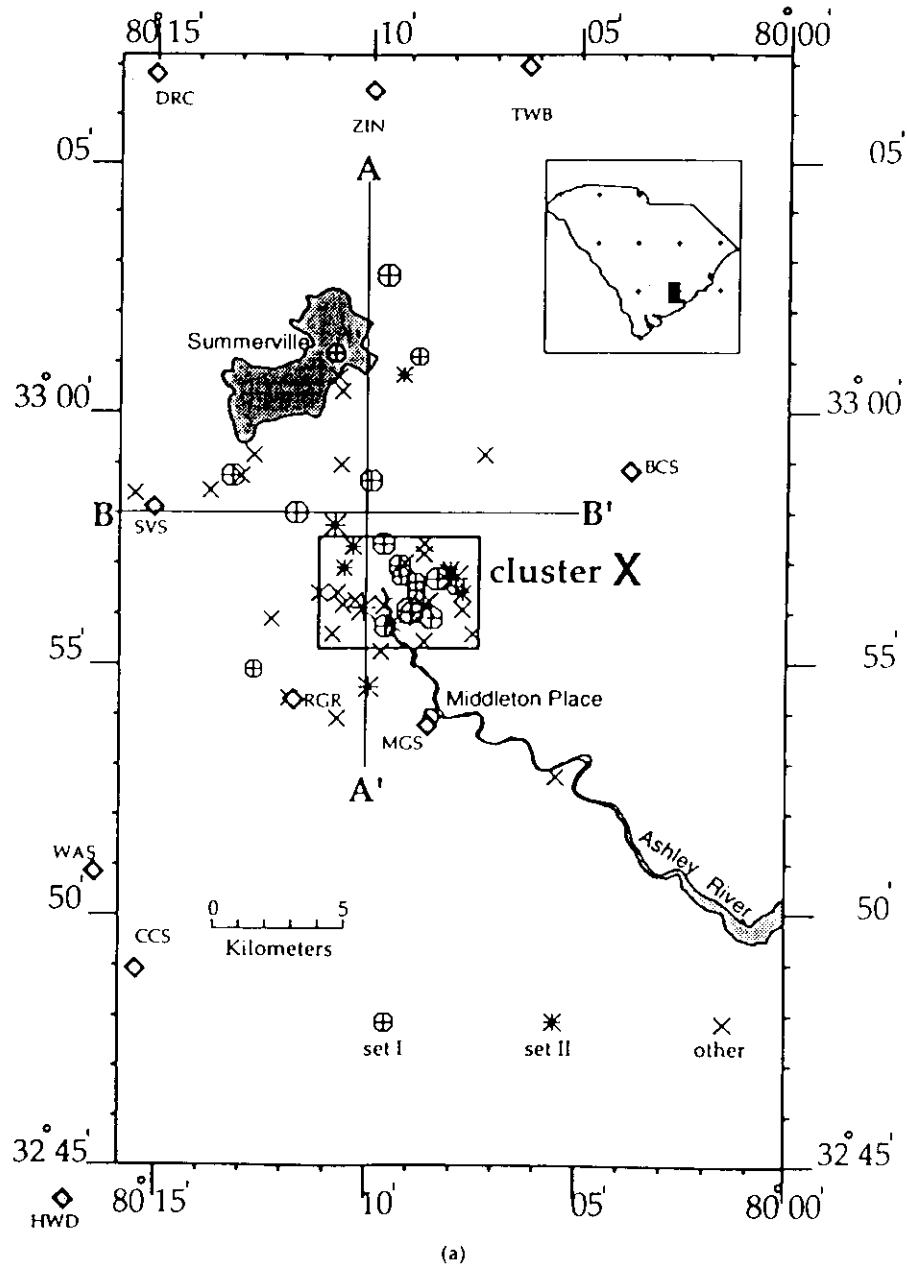
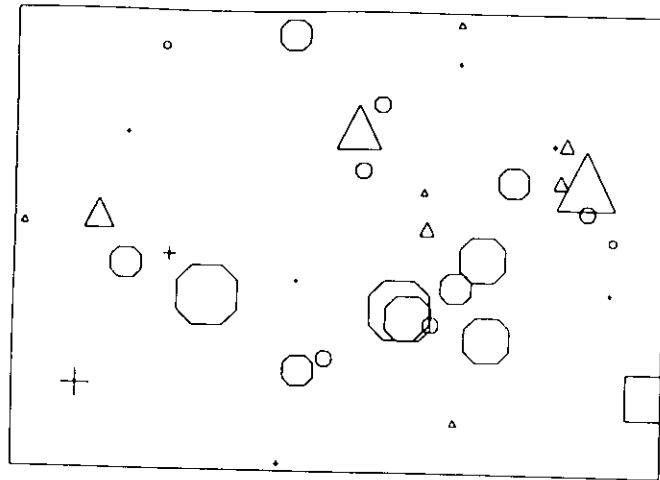
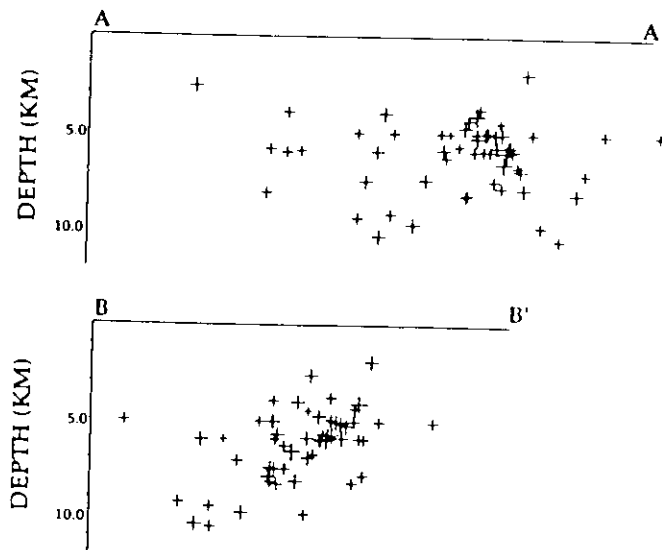


FIG. 1a. Epicenters of earthquakes recorded in MPSSZ between 1980 and 1991. Circles with vertical crosses and asterisks represent events in sets I and II, respectively; crosses—other events; diamonds—seismic stations. 1b. Epicenters in the cluster X according to their magnitudes (smallest < 1.0 and the largest symbol > 3.0) and focal depths (square < 3 km; triangle 3 to 5 km; octagon 5 to 7 km; vertical cross > 7 km). 1c. Distribution of seismicity along N-S (top) and W-E (bottom) cross sections.



cluster X

(b)



(c)

FIG. 1. (Continued)

FAULT PLANE SOLUTIONS

Computer programs FPFIT and FPLOT (Reasenber and Oppenheimer, 1985) were used to compute and plot the FPS. The locations listed in Table 2 were relocated using the HYPOINVERSE (Klein, 1989) and the output was input into FPFIT which computes the solutions based on the polarity data. The number of well recorded first motion polarities for these earthquakes varied from as few as four to as high as 15. The program FPFIT output gives a field of P - and T -axes. For well-constrained solutions the field is narrow (10° by 10° on the stereo net) whereas for unconstrained solutions, it can vary greatly (up to 30° by 90°). The P - and T -axes clusters are shown for only the CFPS in the

TABLE 2
HYPO71 SUMMARY OF THE EARTHQUAKES RELOCATED (WITH CORRESPONDING SET NUMBERS)

Event	Date y/m/d	Origin	Lat N	Long W	Dep	Mag	No	Gap	DM	RMS	ERH	ERZ	QM	Set
01	800901	0544 41.66	32-59.04	80-10.55	7.51	2.86	10	94	7.0	0.09	0.6	0.6	B1	-
02	810319	0433 54.85	32-57.75	80-10.68	7.42	2.25	11	75	6.6	0.06	0.3	0.4	A1	II
03	810326	0912 50.46	32-58.49	80-13.63	9.22	1.44	04	166	2.1	0.01			C1	
04	810608	0510 45.14	32-55.51	80-08.56	5.00	1.18	03	189	3.0	0.03			C1	
05	820115	0754 05.13	32-52.78	80-05.42	5.00	1.72	03	209	17.0	0.02			C1	
06	820201	0725 14.82	32-58.44	80-15.42	5.00	1.93	03	211	17.2	0.95			D1	
07	820301	0333 13.15	32-55.65	80-07.44	1.90	2.82	04	122	17.4	0.02			C1	
08	830322	1200 03.27	32-55.67	80-10.74	7.87	2.10	07	125	7.9	0.11			B1	
09	830626	0744 40.44	32-55.98	80-08.70	5.68	2.00	10	108	3.9	0.06			B1	
10	831106	0902 19.83	32-56.11	80-09.99	6.56	3.29	12	71	4.8	0.08	0.4	0.5	A1	II
11	831106	0904 14.97	32-56.26	80-10.46	5.69	2.11	06	79	5.4	0.07	0.7	1.9	A1	
12	831107	0929 37.00	32-56.31	80-10.21	7.47	1.60	05	152	5.3	0.02	0.3	0.4	C1	
13	840902	2246 43.58	32-55.93	80-12.20	5.94	0.82	06	112	5.8	0.05	0.5	1.1	B1	
14	850519	2329 13.65	33-00.75	80-09.06	6.00	1.64	12	77	8.8	0.10	0.4	0.8	B1	II
15	860309	2349 15.30	32-58.64	80-09.82	3.99	2.25	10	78	8.0	0.10	0.5	1.0	B1	I
16	860508	1545 46.31	33-00.74	80-10.60	3.93	1.44	06	102	8.3	0.02	0.2	0.9	B1	
17	860613	1348 21.92	33-00.45	80-10.53	5.93	1.02	06	222	8.1	0.06	1.6	3.2	C1	
18	860817	2036 32.73	32-57.05	80-09.00	5.67	1.69	06	113	5.9	0.05	1.1	2.4	B1	
19	860917	0933 49.48	32-56.01	80-08.83	5.70	2.75	09	154	5.3	0.08	0.5	0.6	B1	I
20	871006	1742 23.48	32-56.45	80-08.73	4.91	1.93	10	82	4.8	0.06	0.3	0.6	A1	I
21	880123	0157 16.30	32-56.05	80-08.88	5.97	3.29	16	82	4.1	0.04	0.2	0.2	A1	I
22	880430	1937 39.94	33-01.11	80-08.70	5.84	1.72	07	134	8.6	0.05	0.5	1.5	B1	I
23	880530	2311 34.99	32-54.90	80-12.58	10.47	1.32	06	98	1.7	0.02	0.3	0.4	B1	I
24	880623	1205 07.85	32-58.74	80-13.10	10.35	2.00	09	83	3.0	0.06	0.4	0.7	A1	I
25	881027	0347 05.47	32-56.86	80-08.01	8.17	1.18	05	139	5.6	0.04	0.9	2.0	C1	
26	881130	1358 55.75	32-59.21	80-12.62	9.41	1.64	07	180	4.1	0.07	0.9	0.8	C1	
27	881213	0301 01.27	32-56.68	80-08.24	5.23	2.41	12	172	6.7	0.07	0.5	0.5	B1	I
28	890102	1635 16.29	32-56.30	80-08.41	5.07	2.72	12	84	4.5	0.07	0.3	0.6	A1	
29	890422	0929 39.49	32-56.19	80-09.48	4.44	0.82	05	128	4.6	0.01	0.2	0.4	C1	
30	890602	0504 33.78	32-55.75	80-09.46	6.89	2.03	14	80	3.8	0.04	0.2	0.2	A1	I
31	890606	1606 21.52	32-54.37	80-11.75	7.06	1.02	04	224	0.2	0.16			C1	
32	890608	0852 17.35	32-55.81	80-09.31	6.71	1.64	15	81	3.8	0.04	0.2	0.2	A1	II
33	891020	0555 50.90	32-57.25	80-08.56	5.00	0.82	03	206	6.2	0.03			C1	
34	891102	0758 04.84	32-56.46	80-11.05	5.00	1.02	05	132	3.8	0.12	2.6	4.4	D1	
35	900107	1613 16.38	32-58.00	80-11.59	9.74	2.05	09	77	5.1	0.05	0.3	0.3	A1	I
36	900207	0741 39.95	32-54.55	80-09.86	8.10	2.77	12	91	2.5	0.07	0.4	0.4	B1	II
37	900218	1209 39.51	32-57.38	80-09.51	5.86	2.05	09	92	6.4	0.11	0.8	1.2	B1	I
38	900511	1823 34.28	32-56.50	80-10.62	5.00	2.45	10	77	4.1	0.22	1.3	2.1	B1	-
39	900602	0257 41.38	32-56.16	80-08.56	5.01	2.48	06	122	4.2	0.06	2.2	4.9	B1	II
40	900602	1739 15.99	32-53.97	80-10.64	5.00	1.56	04	197	3.4	0.08			C1	-
41	900618	1003 33.30	32-56.94	80-09.13	4.71	2.75	11	102	5.8	0.10	0.6	1.0	B1	I
42	900818	1148 02.29	32-56.63	80-08.75	3.75	1.44	06	113	5.1	0.01	0.2	0.6	B1	I
43	900818	2246 43.92	32-55.91	80-08.38	5.86	2.67	08	160	5.8	0.04	0.4	0.7	B1	I
44	901009	1653 37.05	32-56.69	80-07.97	5.00	1.64	03	265	5.3	0.02			C1	
45	901113	1522 12.86	32-56.70	80-07.82	4.07	3.29	13	133	5.3	0.10	0.6	0.9	B1	II
46	901215	0929 14.43	32-55.30	80-09.57	9.81	1.12	06	93	3.2	0.02	0.3	0.6	B1	
47	910115	2223 33.54	32-56.87	80-07.94	4.32	1.69	07	128	5.6	0.03	0.3	0.9	B1	II
48	910207	0845 27.27	32-56.14	80-07.67	7.80	1.32	06	146	4.4	0.01	0.2	0.4	B1	
49	910218	2045 10.48	32-57.32	80-10.25	6.27	1.44	08	82	5.7	0.02	0.2	0.4	A1	II
50	910305	1146 11.68	33-02.73	80-09.41	2.61	2.00	07	97	9.2	0.03	0.3	1.1	B1	I
51	910327	2204 47.78	33-01.18	80-10.69	8.12	1.72	09	92	8.7	0.04	0.3	0.9	B1	I
52	910423	2039 49.03	32-56.54	80-07.81	5.90	1.72	07	136	5.0	0.04	0.6	1.2	B1	I
53	910424	0342 21.85	32-56.90	80-10.46	8.26	1.44	07	80	4.9	0.04	0.4	0.5	A1	II
54	910517	1227 53.14	32-56.40	80-07.66	5.93	1.44	07	142	4.8	0.04	0.4	0.8	B1	II
55	910602	0605 34.65	32-58.80	80-12.93	5.97	2.05	08	112	8.3	0.07	0.5	2.0	B1	-
56	910824	0323 37.83	32-56.73	80-09.10	5.94	1.54	08	104	5.4	0.03	0.3	0.6	B1	I
57	911028	0653 25.35	32-57.44	80-08.56	5.00	1.18	03	210	6.6	0.16			C1	
58	911117	0632 11.68	32-59.22	80-07.16	5.00	1.02	04	148	5.1	0.01			C1	

figures due to space constraints, but were considered for all the events in the analysis. For events where the polarity data were insufficient to constrain a single focal mechanism, multiple and/or unconstrained solutions were obtained. CFPS were obtained by grouping their phase data in a manner described below.

Of the 58 events, FPS were obtained for 35, each with 6 or more polarities and with location qualities A or B (Table 2). Of these, eleven events with eight or more polarities yielded constrained single event fault plane solutions (SFPS). SFPS for these events (#2, 10, 20, 21, 24, 30, 32, 41, 43, 45, and 56) are shown in Figure 2a to k and are discussed later. FPS for the remaining events are shown in Figure 3a to x. As the data were inadequate to constrain a single focal mechanism, multiple solutions were obtained for 15 events. The FPS for five events (#1, 28, 38, 48, and 55) suggested normal faulting. From our knowledge of the tectonics of the area, the MPSSZ area is under a compressional stress regime. This is based on *in situ* measurements and evidence of uplift in the releveling data (see e.g., Talwani, 1986). These events probably represent kinematic adjustments on small faults in response to movements on other faults. These events were therefore not used in developing CFPS. The polarity data for the event #16 did not fit any of the CFPS and were not used. The polarity data for the remaining 18 events (#14, 15, 19, 22, 23, 27, 35-37, 39-42, 47, 49-54) were used to obtain CFPS.

RESULTS

SFPS

In the period between September 1980 and November, 1991, there were three events with $M_d \geq 3.0$ (event #10, 21, and 45, Table 2). Single fault plane mechanisms, as described in the following section, were obtained for these as well as for eight other events with magnitudes between 0.8 and 2.9.

The $M_d = 3.3$, 6 November 1983 event (#10) was well recorded on stations of South Carolina, Georgia Tech., and Southern Appalachian Seismic Networks. It was bracketed by two teleseisms on 3 November 1983 and 22 November 1983 that were associated with impulsive first arrivals on the regional networks and were used to check the polarities of the stations in the South Carolina network. The FPS (Figure 2b) suggests an oblique strike-slip motion, on a N35°E plane dipping 40°NW. The SFPS for the event #2 also suggests a right lateral strike-slip motion with a large thrust component.

$M_d = 3.3$ 23 January 1988, event (#21) was the largest instrumentally recorded in MPSSZ after the 1983 event. The FPS for this event is shown in Figure 2d. The solution suggests reverse faulting on a N25°W striking plane with a 71°SW dip. The sense of motion associated with events #20, 24, 30, 41, 43 and 56 is also predominantly reverse in nature and occurs along NW trending and SW dipping fault planes. Individually, however, these solutions vary from pure thrust (#30) to thrusting with a large strike-slip component (#41).

The $M_d = 3.2$ earthquake (#45) that occurred on 11 November 1990 is the latest of the larger events in MPSSZ. This event was recorded on a number of stations, and its SFPS is shown in Figure 2j. It suggests almost pure reverse faulting on a N17°W striking fault plane dipping 49°W. The SFPS for the event #32 was associated with right lateral strike-slip motion on a N10°W striking fault plane.

(8)

QM Set

B1 -
 A1 II
 C1 -
 C1 -
 D1 -
 C1 -
 B1 -
 B1 -
 A1 II
 A1 -
 C1 -
 B1 -
 B1 II
 B1 I
 B1 -
 C1 -
 B1 -
 B1 I
 A1 I
 A1 I
 B1 I
 B1 I
 A1 I
 C1 -
 C1 -
 B1 I
 A1 -
 C1 -
 A1 II
 C1 -
 D1 -
 A1 I
 B1 II
 B1 I
 B1 -
 B1 II
 C1 -
 B1 I
 B1 I
 C1 -
 B1 II
 B1 II
 A1 II
 B1 I
 B1 I
 B1 I
 A1 II
 B1 II
 B1 -
 B1 I
 C1 -
 C1 -

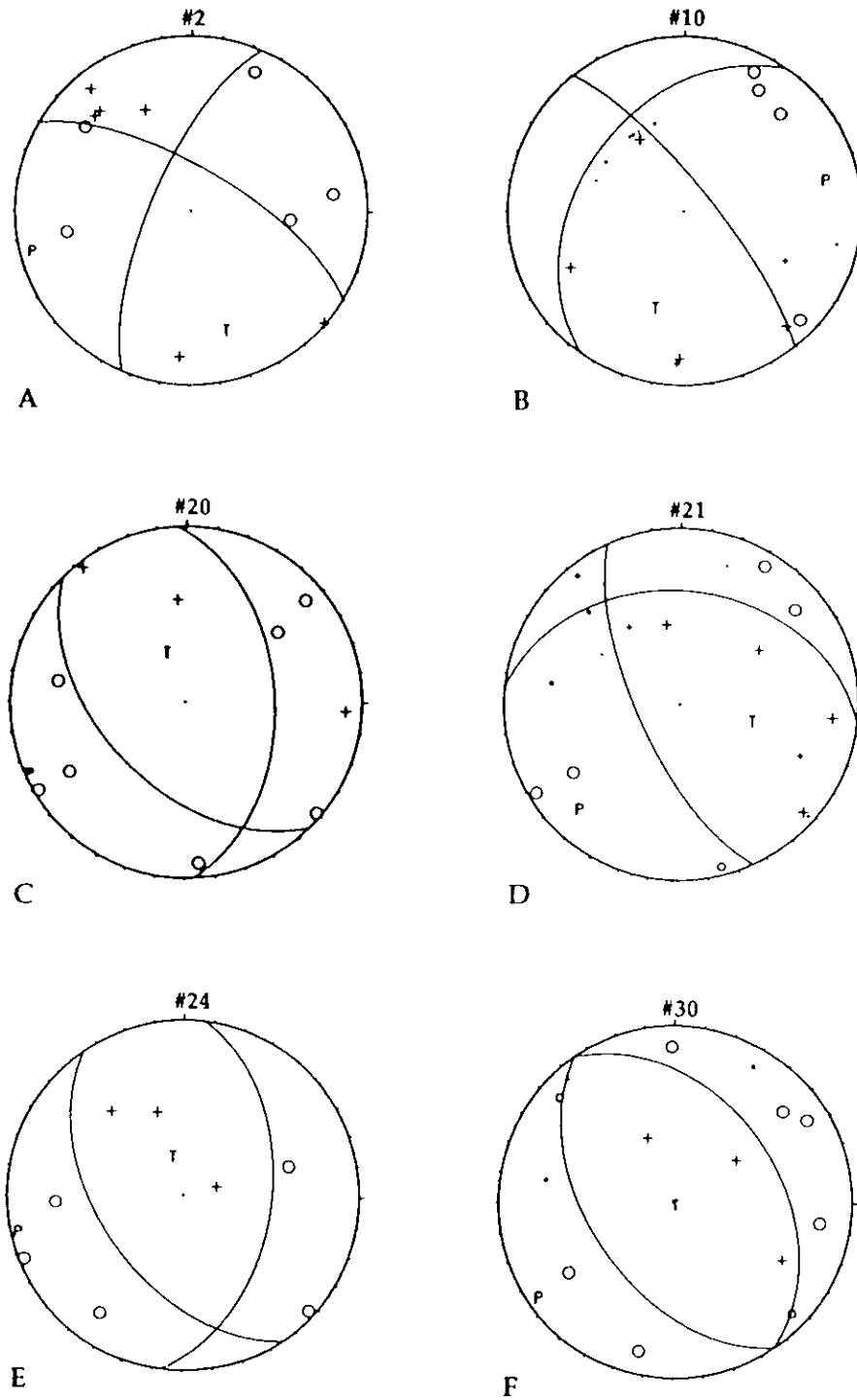
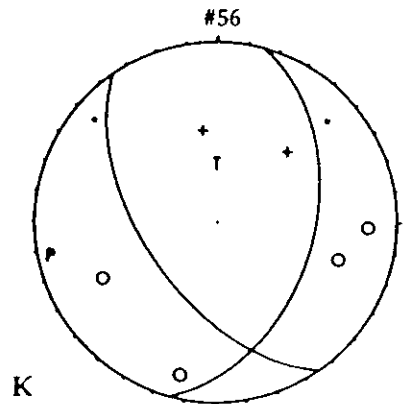
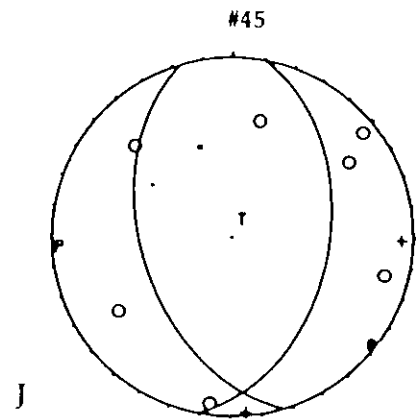
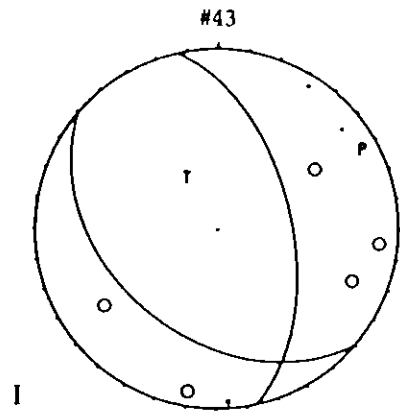
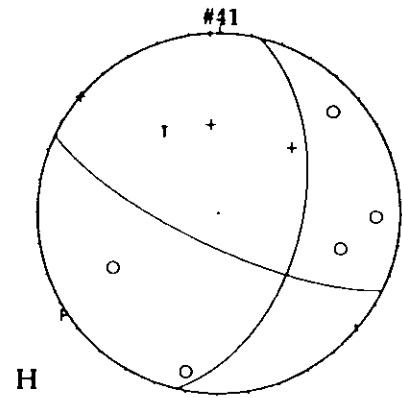
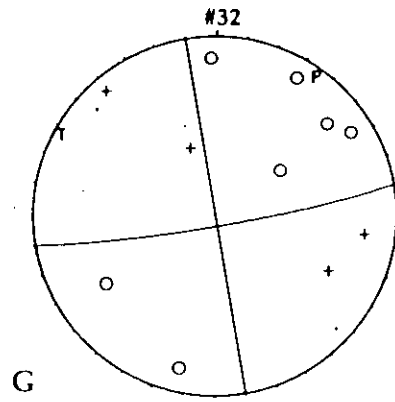


FIG. 2a-k. SFPS for events #2, 10, 20, 21, 24, 30, 32, 41, 43, 45, and 56. Circles and vertical crosses indicate dilatational and compressional first arrivals, respectively.



I vertical

FIG. 2. (Continued)

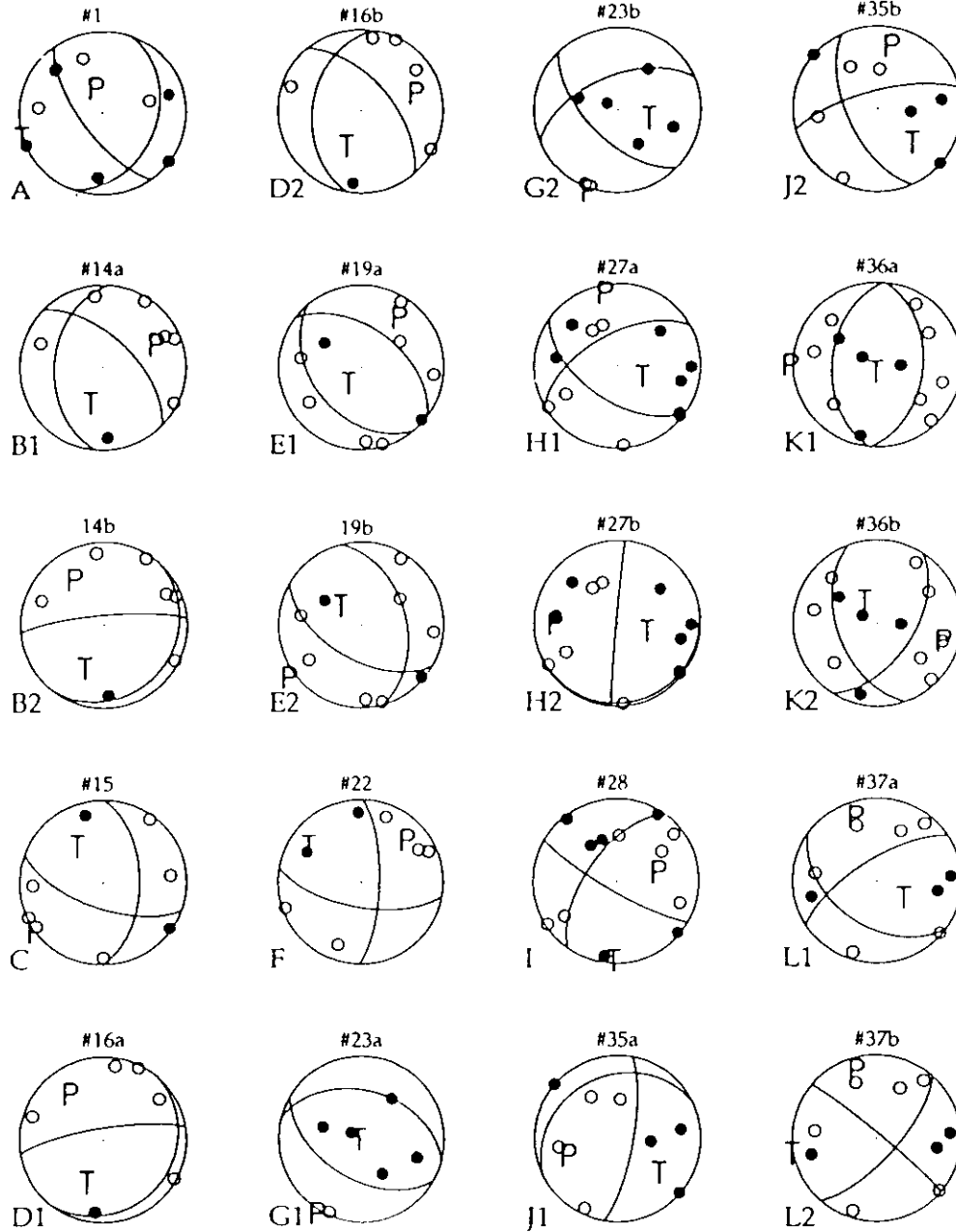


FIG. 3a-x. SFPS for events #1, 14, 15, 16, 19, 22, 23, 27, 28, 35, 36, 37, 38, 39, 42, 47, 48, 49, 50, 51, 52, 53, 54, and 55. Open and solid circles indicate dilatational and compressional first arrivals, respectively. Note many events have multiple solutions.

Thus for the 11 events for which SFPS were obtained, two (#2 and 10) were associated with predominantly right lateral slip motion on NNE-SSW striking fault planes, two (#32 and 45) were associated with faulting on a N-S fault plane, and the remaining with predominantly reverse faulting on NW-SE striking and SW dipping planes. The slip vectors associated with these events

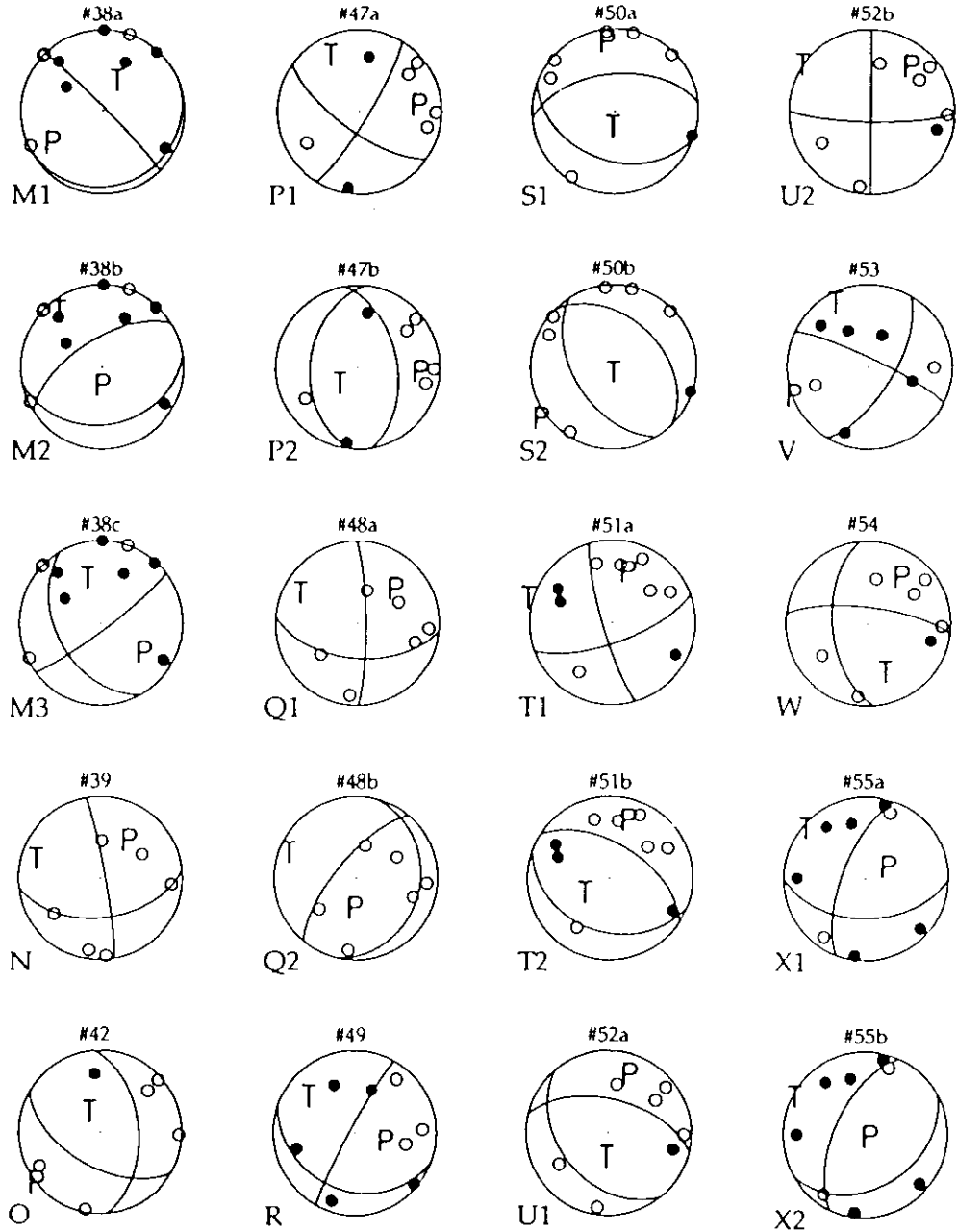


FIG. 3. (Continued)

9, 50, 51, 52, 53, 54, 55, 56, 57, 58, 59, 60, 61, 62, 63, 64, 65, 66, 67, 68, 69, 70, 71, 72, 73, 74, 75, 76, 77, 78, 79, 80, 81, 82, 83, 84, 85, 86, 87, 88, 89, 90, 91, 92, 93, 94, 95, 96, 97, 98, 99, 100, 101, 102, 103, 104, 105, 106, 107, 108, 109, 110, 111, 112, 113, 114, 115, 116, 117, 118, 119, 120, 121, 122, 123, 124, 125, 126, 127, 128, 129, 130, 131, 132, 133, 134, 135, 136, 137, 138, 139, 140, 141, 142, 143, 144, 145, 146, 147, 148, 149, 150, 151, 152, 153, 154, 155, 156, 157, 158, 159, 160, 161, 162, 163, 164, 165, 166, 167, 168, 169, 170, 171, 172, 173, 174, 175, 176, 177, 178, 179, 180, 181, 182, 183, 184, 185, 186, 187, 188, 189, 190, 191, 192, 193, 194, 195, 196, 197, 198, 199, 200, 201, 202, 203, 204, 205, 206, 207, 208, 209, 210, 211, 212, 213, 214, 215, 216, 217, 218, 219, 220, 221, 222, 223, 224, 225, 226, 227, 228, 229, 230, 231, 232, 233, 234, 235, 236, 237, 238, 239, 240, 241, 242, 243, 244, 245, 246, 247, 248, 249, 250, 251, 252, 253, 254, 255, 256, 257, 258, 259, 260, 261, 262, 263, 264, 265, 266, 267, 268, 269, 270, 271, 272, 273, 274, 275, 276, 277, 278, 279, 280, 281, 282, 283, 284, 285, 286, 287, 288, 289, 290, 291, 292, 293, 294, 295, 296, 297, 298, 299, 300, 301, 302, 303, 304, 305, 306, 307, 308, 309, 310, 311, 312, 313, 314, 315, 316, 317, 318, 319, 320, 321, 322, 323, 324, 325, 326, 327, 328, 329, 330, 331, 332, 333, 334, 335, 336, 337, 338, 339, 340, 341, 342, 343, 344, 345, 346, 347, 348, 349, 350, 351, 352, 353, 354, 355, 356, 357, 358, 359, 360, 361, 362, 363, 364, 365, 366, 367, 368, 369, 370, 371, 372, 373, 374, 375, 376, 377, 378, 379, 380, 381, 382, 383, 384, 385, 386, 387, 388, 389, 390, 391, 392, 393, 394, 395, 396, 397, 398, 399, 400, 401, 402, 403, 404, 405, 406, 407, 408, 409, 410, 411, 412, 413, 414, 415, 416, 417, 418, 419, 420, 421, 422, 423, 424, 425, 426, 427, 428, 429, 430, 431, 432, 433, 434, 435, 436, 437, 438, 439, 440, 441, 442, 443, 444, 445, 446, 447, 448, 449, 450, 451, 452, 453, 454, 455, 456, 457, 458, 459, 460, 461, 462, 463, 464, 465, 466, 467, 468, 469, 470, 471, 472, 473, 474, 475, 476, 477, 478, 479, 480, 481, 482, 483, 484, 485, 486, 487, 488, 489, 490, 491, 492, 493, 494, 495, 496, 497, 498, 499, 500, 501, 502, 503, 504, 505, 506, 507, 508, 509, 510, 511, 512, 513, 514, 515, 516, 517, 518, 519, 520, 521, 522, 523, 524, 525, 526, 527, 528, 529, 530, 531, 532, 533, 534, 535, 536, 537, 538, 539, 540, 541, 542, 543, 544, 545, 546, 547, 548, 549, 550, 551, 552, 553, 554, 555, 556, 557, 558, 559, 560, 561, 562, 563, 564, 565, 566, 567, 568, 569, 570, 571, 572, 573, 574, 575, 576, 577, 578, 579, 580, 581, 582, 583, 584, 585, 586, 587, 588, 589, 590, 591, 592, 593, 594, 595, 596, 597, 598, 599, 600, 601, 602, 603, 604, 605, 606, 607, 608, 609, 610, 611, 612, 613, 614, 615, 616, 617, 618, 619, 620, 621, 622, 623, 624, 625, 626, 627, 628, 629, 630, 631, 632, 633, 634, 635, 636, 637, 638, 639, 640, 641, 642, 643, 644, 645, 646, 647, 648, 649, 650, 651, 652, 653, 654, 655, 656, 657, 658, 659, 660, 661, 662, 663, 664, 665, 666, 667, 668, 669, 670, 671, 672, 673, 674, 675, 676, 677, 678, 679, 680, 681, 682, 683, 684, 685, 686, 687, 688, 689, 690, 691, 692, 693, 694, 695, 696, 697, 698, 699, 700, 701, 702, 703, 704, 705, 706, 707, 708, 709, 710, 711, 712, 713, 714, 715, 716, 717, 718, 719, 720, 721, 722, 723, 724, 725, 726, 727, 728, 729, 730, 731, 732, 733, 734, 735, 736, 737, 738, 739, 740, 741, 742, 743, 744, 745, 746, 747, 748, 749, 750, 751, 752, 753, 754, 755, 756, 757, 758, 759, 760, 761, 762, 763, 764, 765, 766, 767, 768, 769, 770, 771, 772, 773, 774, 775, 776, 777, 778, 779, 780, 781, 782, 783, 784, 785, 786, 787, 788, 789, 790, 791, 792, 793, 794, 795, 796, 797, 798, 799, 800, 801, 802, 803, 804, 805, 806, 807, 808, 809, 810, 811, 812, 813, 814, 815, 816, 817, 818, 819, 820, 821, 822, 823, 824, 825, 826, 827, 828, 829, 830, 831, 832, 833, 834, 835, 836, 837, 838, 839, 840, 841, 842, 843, 844, 845, 846, 847, 848, 849, 850, 851, 852, 853, 854, 855, 856, 857, 858, 859, 860, 861, 862, 863, 864, 865, 866, 867, 868, 869, 870, 871, 872, 873, 874, 875, 876, 877, 878, 879, 880, 881, 882, 883, 884, 885, 886, 887, 888, 889, 890, 891, 892, 893, 894, 895, 896, 897, 898, 899, 900, 901, 902, 903, 904, 905, 906, 907, 908, 909, 910, 911, 912, 913, 914, 915, 916, 917, 918, 919, 920, 921, 922, 923, 924, 925, 926, 927, 928, 929, 930, 931, 932, 933, 934, 935, 936, 937, 938, 939, 940, 941, 942, 943, 944, 945, 946, 947, 948, 949, 950, 951, 952, 953, 954, 955, 956, 957, 958, 959, 960, 961, 962, 963, 964, 965, 966, 967, 968, 969, 970, 971, 972, 973, 974, 975, 976, 977, 978, 979, 980, 981, 982, 983, 984, 985, 986, 987, 988, 989, 990, 991, 992, 993, 994, 995, 996, 997, 998, 999, 1000

were striking fault segments with different strike and dip directions rather than a single major fault. Nodal plane data obtained for the SFPS are summarized in Table 3.

also vary in both azimuth and plunge directions. These observations imply that the earthquakes are associated with short fault segments with different strike and dip directions rather than a single major fault. Nodal plane data obtained for the SFPS are summarized in Table 3.

TABLE 3
FAULT PLANE SOLUTIONS

	Nodal Plane 1		Nodal Plane 2(*)		P axis	
	Strike	Dip	Strike	Dip	Azimuth	Plunge
SFPS						
Event#						
2	300	70	23	72	253	2
10	141	78	35	40	78	21
20	357	49	315	50	246	1
21	96	35	335	71	223	20
24	7	49	225	51	257	2
30	325	40	325	50	235	5
32	80	95	350	90	36	3
41	13	52	295	75	238	16
43	347	77	310	40	60	6
45	10	56	343	49	266	2
56	15	45	225	58	259	7
CFPS						
set						
IA	5	56	277	73	236	15
IB	304	46	290	44	25	2
IC	310	54	340	50	235	5
IIA	295	80	25	90	250	9
IIB	5	50	350	41	89	5

* Preferred fault planes.

CFPS

Obtaining CFPS involves making some simplifying assumptions and some degree of subjectivity. The usual assumption is that events included in a CFPS occurred on a single fault. For the small events used to make CFPS the fault dimensions are small and we therefore seek events for which the polarity data cluster about a common average solution. The following procedure was adopted to obtain CFPS (the procedure is similar to that used by Mendiguren (1980), Rastogi and Talwani (1980) and Talwani (1982) among others).

Only well-located data (see earlier section) were used, i.e., the depths were reliable and the differences in focal mechanisms were not due to poor accuracy in depth estimations, but due to inherent differences in the mechanisms themselves.

The data were segregated according to the polarities at a given station. The polarities at the stations ZIN and TWB were particularly diagnostic—being either compressions or dilatations. These stations are located to the north of the main cluster (Fig. 1a) and differences in polarities for different events coming from essentially the same location suggested multiple mechanisms.

Because most of the events were located in a cluster, they did not define a continuous rupture zone. Hence the hypocentral distribution of events used in a CFPS could not be used to discern the fault plane. In choosing a nodal plane we adopted the following procedure. The events used in obtaining a CFPS were plotted in cross sections along and perpendicular to the strikes of the two nodal planes. It was found that when there were adequate data to define a tabular zone (in cross section) an unambiguous choice of the fault plane could be made.

Additionally, the data used in any CFPS were viewed in stereographic projections. Using these criteria, the SW and westerly dipping nodal planes were chosen as the fault planes.

Polarity data for the 18 events for which we obtained unconstrained or multiple SFPS were analyzed to obtain CFPS. For 11 events in set I, a dilatational first motion was observed for ZIN (TWB). For the seven events in set II, ZIN (TWB) was compressional in five cases. Nodal plane data obtained for the CFPS are summarized in Table 3.

Set I

Eleven events with similar unconstrained solutions (#15, 19, 22, 23, 27, 35, 37, 42, 50, 51, and 52) were combined to obtain the CFPS shown in Figure 4a. This solution represents the average solution for all the first arrival data from these events and contains 87 first arrivals with 17 inconsistencies. The solution gives a predominantly reverse faulting mechanism with a small strike slip component. The strike of SW dipping fault planes of individual events used in compositing varied between 280° and 340° , thus accounting for the large number of inconsistencies in the CFPS. The range in the strike direction of the SW dipping fault plane in the SFPS of #20, 21, 24, 30, 41, 43, and 56 also varied between 295° and 335° . Thus the 11 events used in the CFPS, combined with these seven events for which we have SFPS, were divided into three subsets according to the strike of the SW dipping planes.

Subset IA

Events #15, 22, 41, 42, and 51 are combined as a subset to produce a CFPS. The strike of the SW dipping plane in the SFPS (for #41) and for at least one of the multiple solutions (for #15, 22, 42, and 51) was between 280° and 295° . The resulting CFPS (Fig. 4b) had two inconsistencies of 39 polarities. It shows a reverse fault mechanism on a $N73^\circ W$ striking fault dipping 73° to SW with some slip component. The *P*-axis for the composite fault plane is oriented $S56^\circ W$ with a plunge of 15° .

Figure 5a shows the epicentral distribution for events of subset IA. The cross section along AA' does not define an obvious fault plane. The events may be associated with two parallel zones, one consisting of events #41, 42, and 15 and the other #22 and 51. From the epicentral distribution we also see that the events 22 and 51 are to the north and outside the main cluster. The data are too sparse to identify the fault planes conclusively. The apparent northwesterly dip (cross section along BB') is not supported by the focal mechanism (Fig. 4b) whereas the other nodal plane dips to the east.

Subset IB

Events, #19, 20, 23, 27, 37, 43, and 52 were combined to seek a CFPS. The strike of the SW dipping plane in the SFPS of #20 and 43 and at least one of the planes in the multiple solutions for events #19, 23, 27, 37, and 52 was between 305° and 320° . The CFPS (Fig. 4c) has 14 inconsistencies of 61 in the polarities. It indicates an almost pure thrust solution on a $N56^\circ W$ striking plane with a $46^\circ SW$ dip. The *P*-axis for this solution has an azimuth of $N25^\circ E$ strike and a 2° plunge. For subset IB events the epicentral distribution and the two cross sections are shown in Figure 5b. In this case, the difference between the two cross sections is very clear. In the section along AA', a 3-km zone dipping $46^\circ SW$

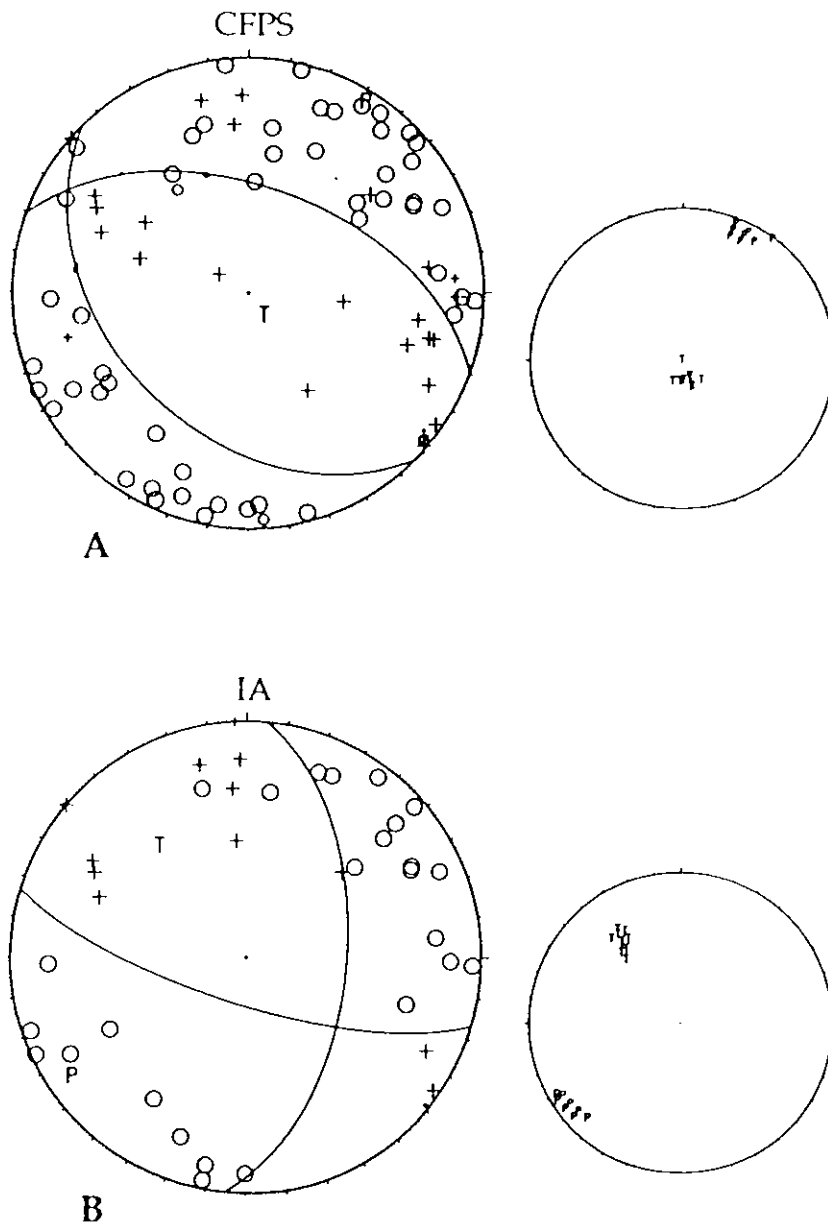


FIG. 4 CFPS for the Set I (ARF). a for events #15, 19, 22, 23, 27, 35, 37, 42, 50, 51 and 52; b, c, and d for the subsets IA, IB, and IC, respectively. Symbols same as in Figure 2 Companion plots show distribution of *P*- and *T*-axes clusters in each case

as indicated by the CFPS, encompasses all the events. The apparent NW dip (section BB') is not supported by the CFPS.

Subset IC

Of the six events (#21, 24, 30, 35, 50, and 56) used to obtain a CFPS, we had SFPS for four. For events 35 and 50 there were multiple solutions with at least

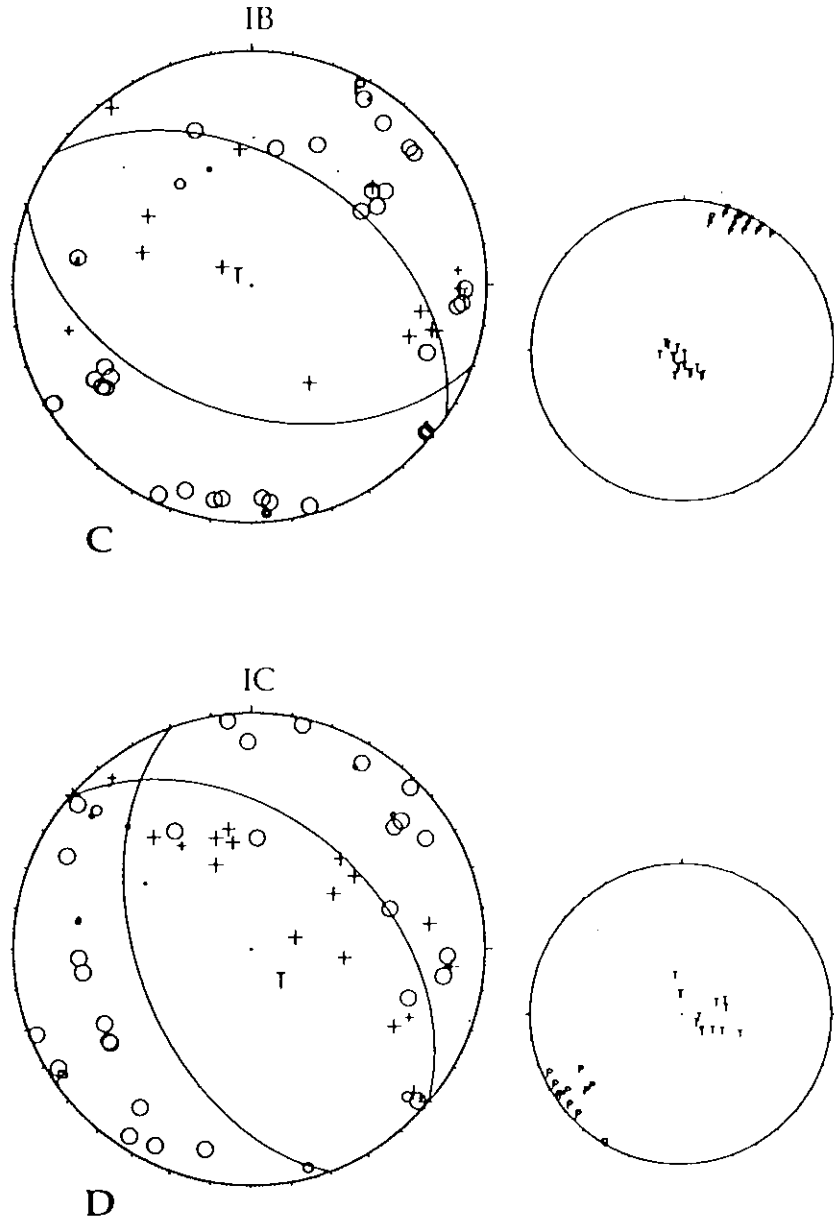


FIG. 4. (Continued)

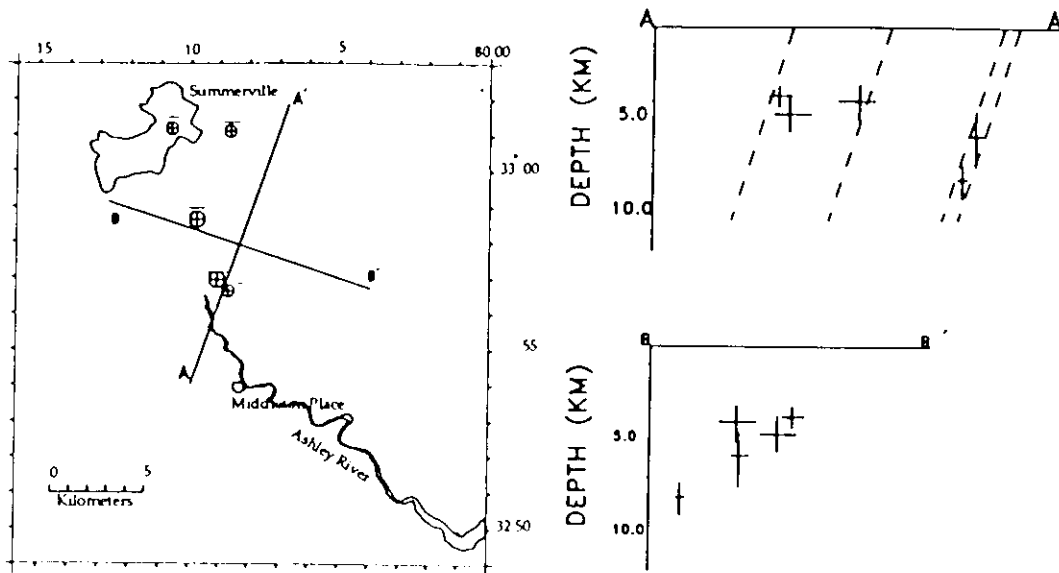
nd 52; b, c,
union plots

NW dip

we had
at least

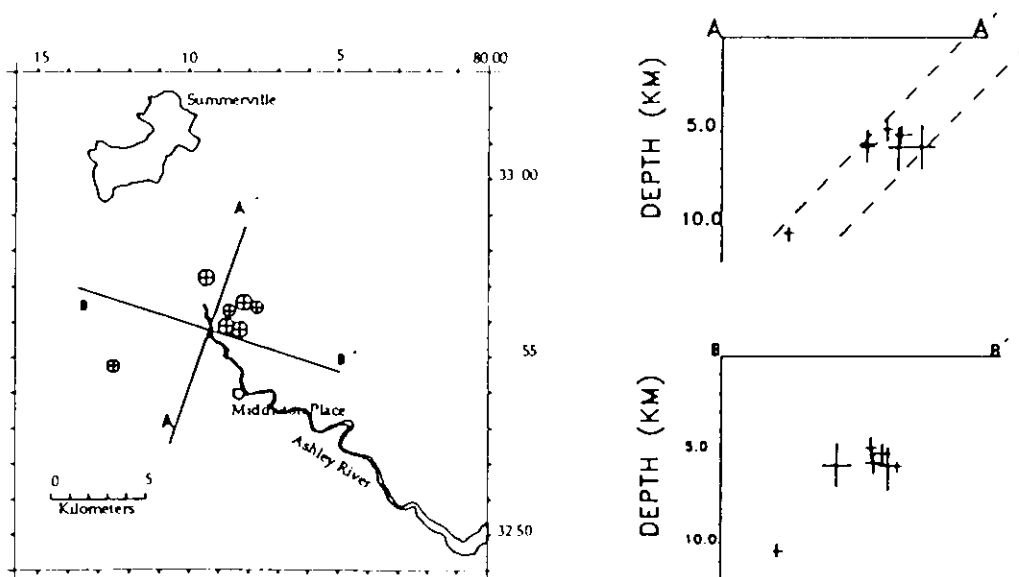
one SW dipping plane with strike between 325° and 340° similar to those in the SFPS. The CFPS (Fig. 4d) represents reverse faulting on a plane striking $N20^\circ W$ and a dip of 50° to the SW. It has 11 of 61 polarity inconsistencies. The P axis has an azimuth of $S55^\circ W$ strike and a 5° plunge. Figure 5c shows the epicentral location of events in subset IC and two cross sections. The cross section along AA', shows that all events can be fit into a zone about 4 km wide dipping $50^\circ SW$, as given by the CFPS.

set IA



(a)

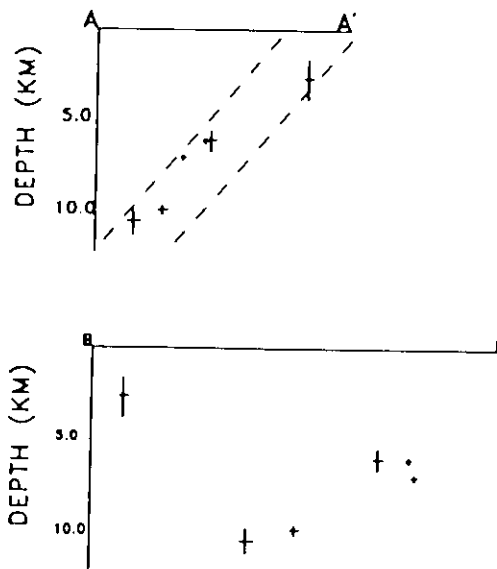
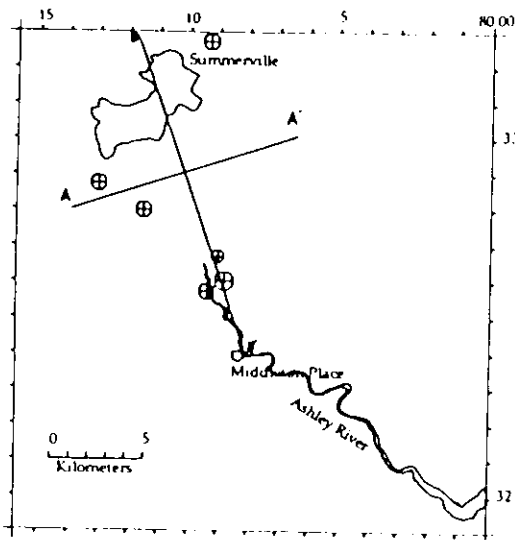
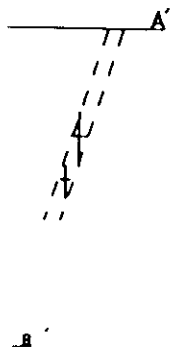
set IB



(b)

FIG. 5a, b, and c. Map view of the epicenters and vertical cross sections (symbol size proportional to errors in hypocentral locations) across (AA') and along (BB') the proposed fault plane for subsets IA, IB, and IC, respectively. Dashed lines indicate southwesterly dipping planes as given by the focal mechanisms in Figure 4b, c, and d.

set IC



(c)

FIG. 5. (Continued)

Set II

Events #14, 36, 39, 45, 49, 53, and 54 were combined to obtain a CFPS shown in Figure 6a. The CFPS contains 49 first arrivals with eight inconsistencies, again suggesting the local perturbations in the fault planes. The sense of motion is right lateral strike slip motion on a NNE trending fault. Most of the events used in the CFPS had westerly dipping fault planes and their strike directions fell into two groups: NNE-SSW and N-S. FPS of single events with similar strike directions were combined to obtain two CFPS.

Subset IIA:

Events #2, 10, 49, and 53 all have similar strike slip solutions, with a nodal plane in each case striking in a N-NE direction. The CFPS obtained by combining these events (Fig. 6b) is associated with almost pure right lateral strike slip along a N25°E striking nodal plane. The solution has 7 inconsistencies of 46 polarities. The azimuth of the P axis is S70°W and its plunge is 9°. Here, we have four closely spaced events, which on the cross sections are too closely spaced to verify the presence of a vertical fault plane, although their location does not preclude it (Fig. 7a).

Subset IIB:

Events #14, 32, 36, 39, 45, 47, and 54 all have a focal plane striking roughly N-S and with most of them dipping to the west. The polarity data for these events were combined to produce a CFPS (Fig. 6c). The solution with 14 inconsistencies in 66 first motions indicates a thrust faulting motion on a N10°W trending fault dipping at 41° to the west, with a small strike slip

proportional
for subsets
given by the

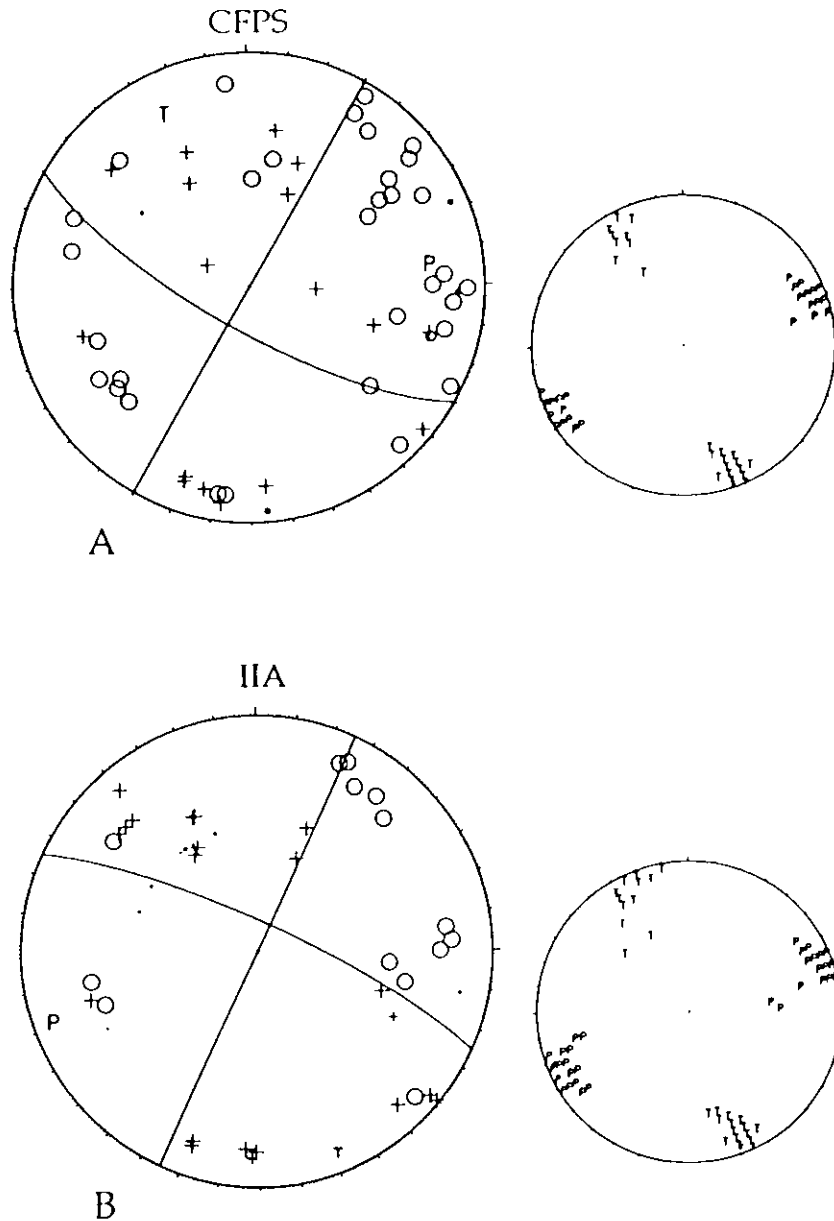


FIG. 6. CFPS for the Set II (WF). a for events #14, 36, 39, 45, 47, 53, and 54. b and c for the subsets IIA and IIB, respectively. Symbols same as in Figure 2. Companion plots show distribution of *P*- and *T*-axes clusters in each case.

component. The *P*-axis has a N89°E azimuth and a 5° plunge. Figure 7b shows the epicentral and cross sectional locations of the events in subset IIB. The cross section across the proposed fault plane (AA') shows a westward dipping fault plane. A 2-km zone dipping 40°W, in agreement with the CFPS (Fig. 6c), encloses hypocenters. These events support thrust faulting with a small strike slip component on a N-S plane dipping about 41° to the west. This N-S fault



and c for the distribution

7b shows The cross dipping fault (Fig. 6c), shall strike N-S fault

HIB

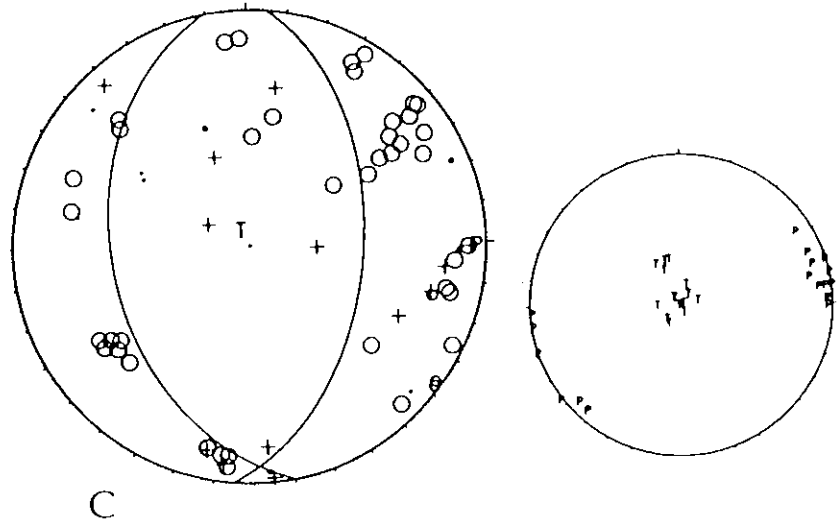


FIG. 6. (Continued)

plane associated with reverse faulting is observed for the first time in MPSSZ and its significance is discussed in the next section.

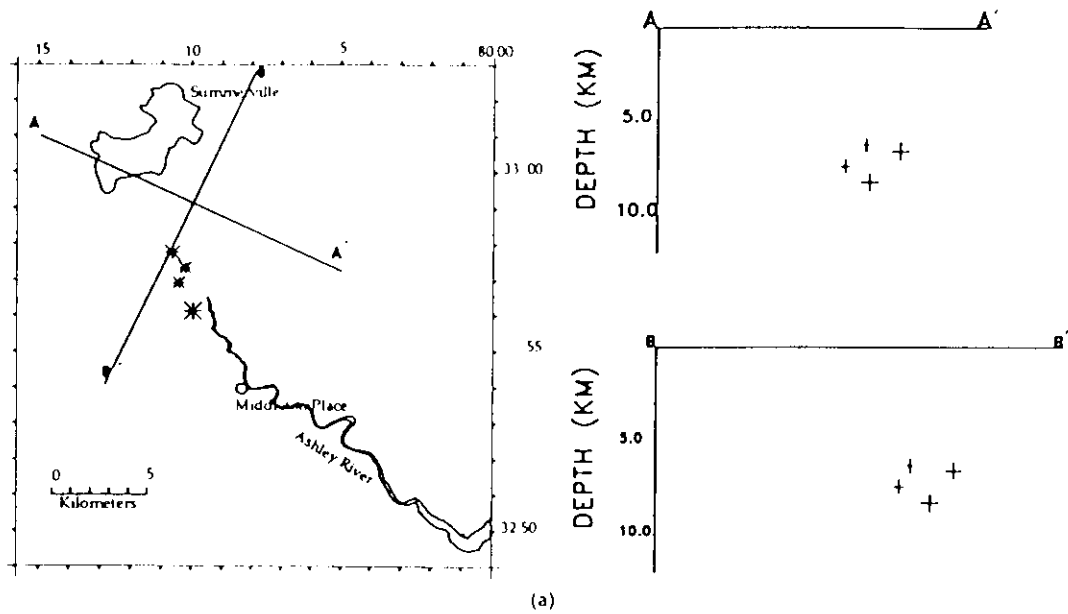
The *P* axes for the 11 SFPS (Fig. 2a-k) and the five CFPS (Figs. 4b-d, 5b and c) are shown in Figure 8. All the *P* axes are oriented in a NE-SW direction and the mean direction N63°E is consistent with earlier estimates, based on seismological (Talwani, 1982) and *in situ* stress (Zoback *et al.*, 1987) estimates of the direction of the maximum horizontal compressive stress in the region.

STEREOGRAPHIC PROJECTIONS

Hypocenters of the events in different subsets (as described in the previous section) were plotted in a 3D space using the program STEREO (German and Johnson, 1981). These plots can be used to view the hypocenters from different angles in 3D space to seek possible alignments. Figure 9a shows all the events plotted in a stereographic projection viewed from a point 15 km above the center of the cluster (32°57'N, 80°10'W). The same events were viewed from a point 15.5 km south of the cluster located 7 km below the surface (Figure 9b). The boxes around the jacks representing the hypocentral locations are parallel to the geographic axes. As can be seen from these stereographic projections, the division of hypocenters into different sets is not very obvious.

Based on the earlier division stereograms were plotted showing earthquakes associated with each set. The stereographic projection of events associated with set I is shown in Figure 10a. The line of view along N70°W is at a depth of 7 km. A cluster of hypocenters is supportive of SW dipping and NW trending fault planes, in general agreement with their CFPS. This supports the choice of SW dipping nodal planes as preferred fault planes (Table 3). The view direction for the set II is along a N-S line at a depth of 7 km from a point 16.6 km south of the center of the cluster (Fig. 10b). Here again the hypocenters define planes dipping to the west in general agreement with the direction of preferred nodal

set IIA



set IIB

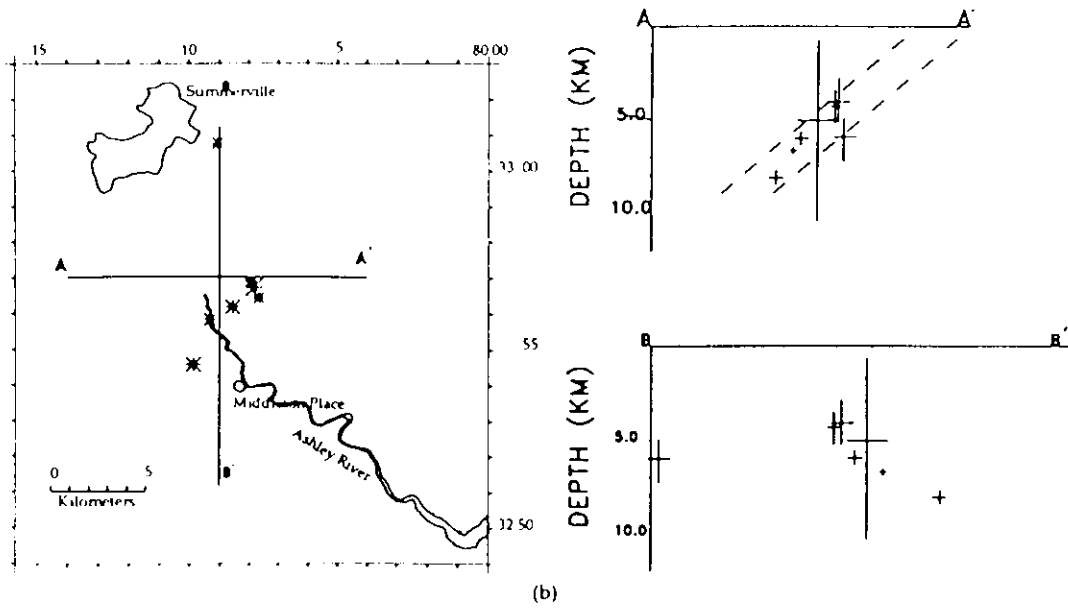


FIG. 7a and b. Map view of the epicenters and vertical cross sections (symbol size proportional to errors in hypocentral locations) across (AA') and along (BB') the proposed fault plane for subsets IIA and IIB, respectively. Dashed lines indicate westerly dipping planes as given by the focal mechanisms in Figure 6c

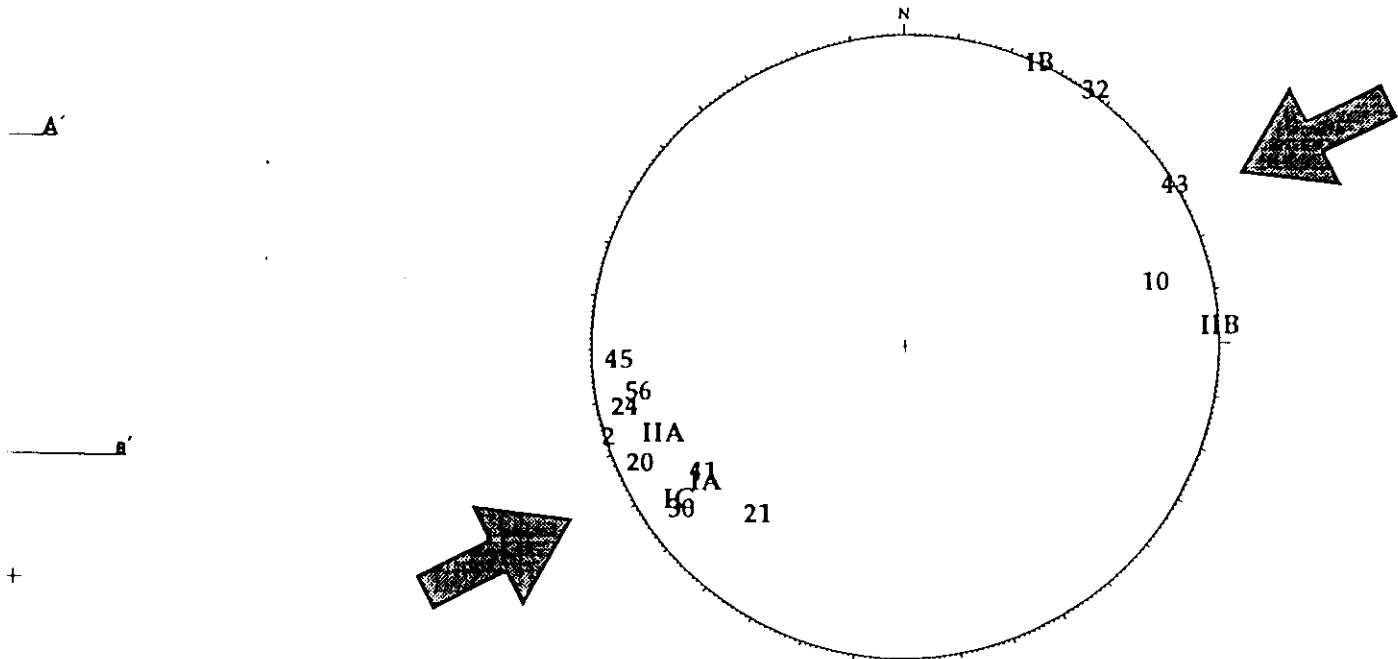


FIG. 8. A comparison of P -axes of 11 SFPS and the five CFPS. The direction of mean P -axis inferred to be the regional $S_{II\max}$ is shown as large arrows oriented $N63^\circ E$. P -axes are shown by event # and IA, IB, IC, IIA, IIB for the five subsets.

planes in the CFPS. In summary, the stereographic projections generally support the CFPS of the subsets.

DISCUSSION AND CONCLUSIONS

MPSSZ is the most active zone seismicity in the Coastal Plain region of South Carolina. In the period between 1980 and 1991, 58 earthquakes varying in magnitude (M_d) between 0.8 and 3.3 were recorded in the MPSSZ. In comparison to the period between 1974 and 1980, there were fewer events in BSZ and none in ARSZ. Temporally, there was a marked increase in activity in 1988 in MPSSZ. Between 1988 and 1991, there were 38 events (Table 2). There were 21 events with magnitude ≥ 2.0 during the study period, of which three were over 3.0. Most of them were felt and occurred throughout the study period. The larger events ($M_d \geq 2.5$) occurred in isolation and were not followed by well-developed aftershock sequences.

The seismicity occurred in a diffuse pattern, with 55 of the 58 events occurring in an area of 11 km by 14 km, bounded by latitudes $32^\circ 54'$ and $33^\circ 01'$ and longitudes $80^\circ 07'$ and $80^\circ 14' W$ (Fig. 1a). Of these, nearly two-thirds (37) occurred in a small region X (Fig. 1b) of 5 km by 6 km, bounded by latitudes $32^\circ 55'$ and $32^\circ 57' N$ and longitudes $80^\circ 07.5'$ and $80^\circ 11' W$. The depth range of the events of all qualities, varied between 1.9 and 10.5 km (Fig. 1c).

Examination of the hypocentral distribution of the events as a function of their magnitude revealed that most (8/10) of the larger events ($M_d \geq 2.5$) were located in the cluster X. The hypocentral depth distribution of the events shows a consistent pattern. Of the 41 events with location qualities of A or B, 29

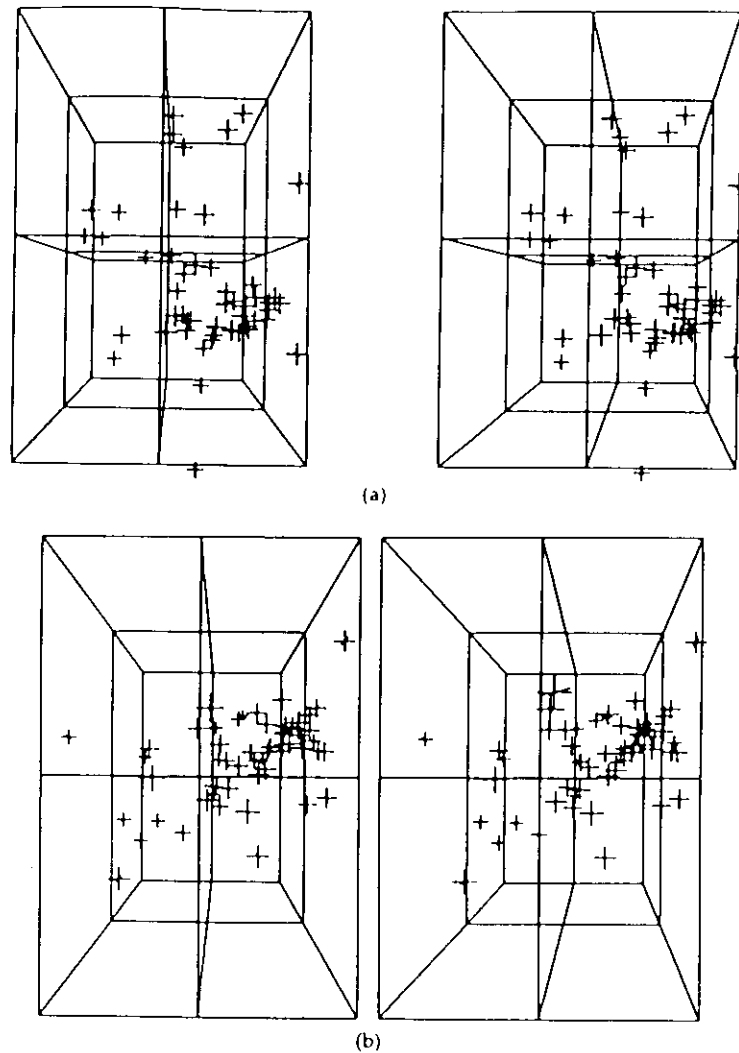


FIG. 9. Stereographic projection of all the hypocenters viewed from (a) a point 15 km above the center of cluster ($32^{\circ}57'N$ and $80^{\circ}10'W$) and (b) from a point 15.5 km south of the cluster center, at a depth of 7 km. Horizontal planes are at 0, 7, and 14 km depths.

events had a hypocentral depth between 3 km and 7 km. Only one event is shallower than 3 km and there are 11 events with depths larger than 7 km. Twenty-two events of these 29 were within the region X and of the 11 deeper events, only 4 were within the region X (Fig. 1b).

Thus, analysis of the hypocentral locations of the earthquakes shows that about $2/3$ of them are located in a dense cluster X and lie between the depths of 3 and 7 km. Also, most of the larger and a few deeper events lie within the cluster.

The epicentral distribution does not show any obvious pattern. In order to infer the structural cause of the earthquakes, the seismicity was divided into sets according to their focal mechanisms. Eleven SFPS and five CFPS were obtained using 35 A and B quality events. The locations of the events in

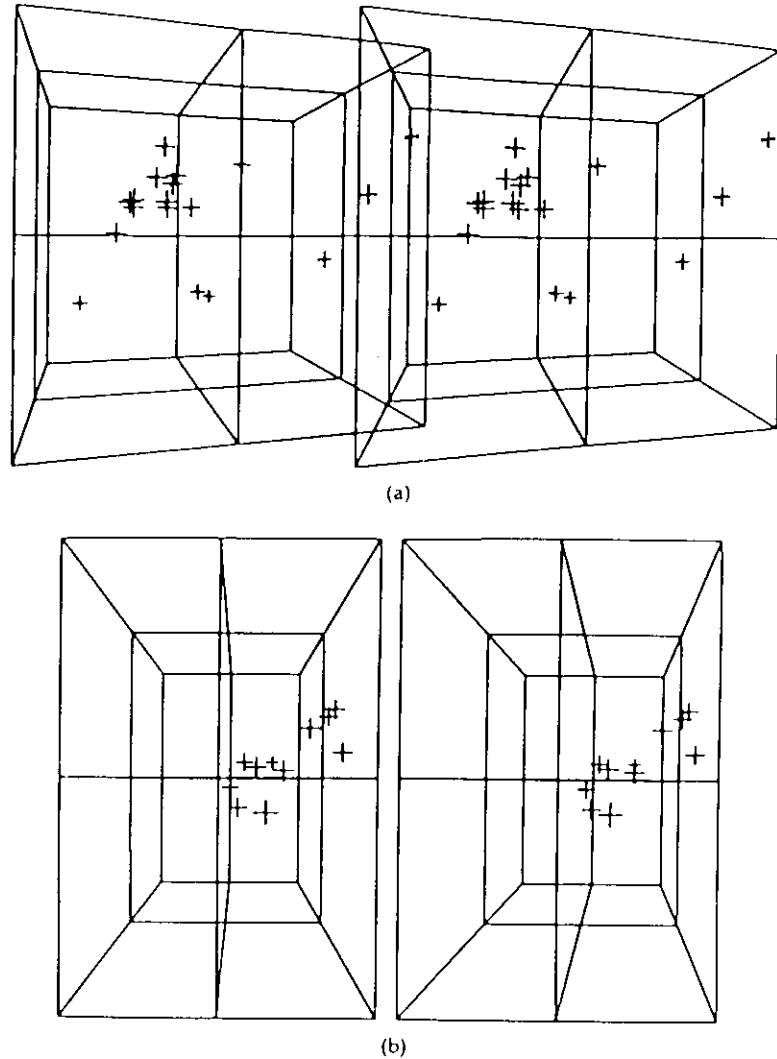


FIG. 10. Stereographic projection of events belonging to (a) ARFZ viewed from a point ($32^{\circ}55'2''N$ and $80^{\circ}W$) 20 km SE of the cluster center and at a depth of 7 km. (b) WFZ viewed from a point 16.6 km south of the cluster center and at a depth of 7 km.

above the
center, at a

event is
in 7 km.
1 deeper

ows that
depths of
within the

order to
ded into
PS were
events in

different sets were examined by plotting them in 3D stereographic projections and in cross sections along and perpendicular to the fault plane inferred from the FPS. The results of this analysis showed that of the 35 events for which FPS were obtained, 23 events favored FPS along NW-SE striking faults and 12 along N-S to NNE-SSW striking fault planes.

For the first set, the strike and dip of the individual FPS varied between $N70^{\circ}W$ and $N20^{\circ}W$ and 40° and $70^{\circ}SW$, respectively. These events were associated with various amounts of reverse faulting with variable amounts of strike-slip motion on fault planes striking NW and dipping to the SW. The FPS suggests compatibility with the Ashley River fault zone. The events were further divided into three subsets, according to their strike and dip. The results of CFPS and cross sections suggest that the ARF zone is not a planar feature.

but is composed of short segments with varying strikes and dips—all generally striking NW and dipping SW. Subsets IA and IB strike \sim N70°W but dip steeply (73°) and moderately (46°) and were associated with large and small components of strike-slip motions. This is to be expected, with $S_{H_{max}}$ oriented ENE-WSW. The fault identified in the FPS of the third subset (IC) is oriented N20°W, about 80° from the $S_{H_{max}}$. It is associated with an almost pure reverse faulting mechanism on planes dipping at about 50°SW.

The second set consists of 11 events with vertical fault planes and the others dipping to the west were oriented NNE-SSW and N-S, respectively. Segregation of these events into two subsets revealed that the subset IIA, oriented NNE-SSW was associated with right-lateral strike slip motion on near vertical fault and subset IIB oriented N-S with oblique faulting with a strong thrust component on a plane dipping about 41°W. These styles of faulting are in general agreement with the anticipated sense of motion on these faults in response to the orientation of $S_{H_{max}}$. These two subsets were classified as belonging to WF zone.

The cluster of intense activity (X) (Fig. 1b) was found to include events that were associated with all the subsets. There is a distinct variation in dips and strikes of the inferred fault planes. The magnitude range (0.8 to 3.3) suggests that the lengths of associated fault segments varied between about 150 m and 1 km. These observations indicate that the rocks in X are severely deformed with short (< 2 km long) fault segments with varying orientations and dips. From these observations we conclude that the seismicity in the cluster X defines the intersection of two fault zones, which we infer to be the ARFZ and WFZ.

ACKNOWLEDGMENTS

We wish to thank K. M. Shedlock, L. T. Long, R. L. Wheeler and the anonymous reviewer for their reviews of an earlier version of this manuscript and D. Oppenheimer and F. Klein for the computer programs. This study was partially funded by the South Carolina Universities Research and Foundation Grant, and U.S. Geological Survey Award No. 1434-92-A-0970.

REFERENCES

- Bollinger, G. A., A. C. Johnston, P. Talwani, L. T. Long, K. M. Shedlock, M. S. Sibol, and M. C. Chapman (1991). Seismicity of the Southeastern United States, 1698-1986, in *Neotectonics of North America*, D. B. Slemmons, E. R. Engdahl, M. D. Zoback, and D. Blackwell, (Editors), Geological Society of America, Boulder Colorado, *Decade Map Volume 1*: 291-308.
- Dewey, J. W. (1985). A Review of Recent Research on the Seismotectonics of the Southeastern Seaboard and an Evaluation of Hypotheses of the 1886 Charleston, South Carolina Earthquake, NUREG/CR-4339, 44 pp.
- German, P. and C. Johnson (1981). A Computer Program for Projecting and Plotting Stereograms, *U.S. Geol. Surv. Open-File Rept. 82-0726*, 74 pp.
- Gohn, G. S. (1983). Editor, Studies Related to the Charleston Earthquake of 1886: Tectonics and Seismicity: *U.S. Geol. Surv. Prof. Paper 1313*, 375 pp.
- Johnston, A. C., D. J. Reinbold and S. I. Brewer (1985). Seismotectonics of the Southern Appalachians, *Bull. Seism. Soc. Am.* **75**, 291-312.
- Klein, F. W. (1989). User's Guide to HYPOINVERSE, a program for VAX computers to solve for Earthquake Locations and Magnitudes, *U.S. Geol. Surv. Open-File Rept. 89-314*, 49 pp.
- Lee, W. H. K. and J. C. Lahr (1975). HYPO71 (Revised): A Computer Program for Determining Hypocenter, Magnitude and First Motion Pattern of Local Earthquakes, *U.S. Geol. Surv. Open-File Rept. 75-311*, 116 pp.
- Mendiguren J. A. (1980). A procedure to resolve areas of different source mechanisms when using the method of composite nodal plane solutions, *Bull. Seism. Soc. Am.* **70**, 985-998.
- Rankin, D. W. (1977). Studies Related to Charleston South Carolina Earthquake of 1886: A Preliminary Report, *U.S. Geol. Surv. Prof. Paper 1028*, p. 204.

- Rastog, B. K. and P. Talwani (1980). Relocation of Koyna Earthquakes, *Bull. Seism. Soc. Am.* **70**, 1849-1868.
- Reasenber, P. A. and D. Oppenheimer (1985). FPFIT, FPPLLOT, FPPAGE. Fortran Computer Programs for Calculating and Displaying Earthquake Fault-Plane Solutions, *U.S. Geol. Surv. Open-File Rept.* 85-739, 47 pp.
- Rhea, S. (1987). Wave conversions from earthquakes and a new velocity model for the South Carolina coastal plain, *Bull. Seism. Soc. Am.* **77**, 2143-2151.
- Shedlock, K. M. (1987). Earthquakes Recorded by South Carolina Seismic Network (1974-1986), *U.S. Geol. Surv. Open-File Rept.* 87-437, 92 pp.
- Shedlock, K. M. (1988). Seismicity in South Carolina, *Seism. Res. Lett.* **59**, 165-171.
- Shedlock, K. M. and S. W. Roecker (1987). Elastic wave velocity structure of the crust and upper mantle beneath the North China basin, *J. Geophys. Res.* **92**, 9319-9325.
- Stihler, S. D. (1985). Seismic Refraction Anisotropy and Seismicity in South Carolina, *M.S. Thesis*, Columbia, University of South Carolina, 102 pp.
- Talwani, P. (1982). Internally consistent pattern of seismicity near Charleston, South Carolina, *Geology* **10**, 654-658.
- Talwani, P. (1985). Current thoughts on the cause of the Charleston, South Carolina earthquakes, *South Carolina Geology* **29**, 19-38.
- Talwani, P. (1986). Seismotectonics of the Charleston region, in Proceedings of the third U.S. National Conference on Earthquake Engineering EERI, Vol. I, 15-24.
- Tarr, A. C. (1977). Recent seismicity near Charleston, South Carolina, and its relationship to the August 31, 1886 earthquake, in Studies Related to Charleston South Carolina Earthquake of 1886: A Preliminary Report, D. W. Rankin, (Editor), *U.S. Geol. Surv. Prof. Paper* 1028, 43-57.
- Tarr, A. C., P. Talwani, S. Rhea, D. Carver and D. Amick (1981). Results of recent South Carolina seismological studies, *Bull. Seism. Soc. Am.*, **71**, 1883-1902.
- Tarr, A. C. and S. Rhea (1983). Seismicity near Charleston, South Carolina, March 1973 to December 1979, in Studies Related to the Charleston, South Carolina Earthquake of 1886: Tectonics and Seismicity, G. S. Gohn, (Editor), *U.S. Geol. Surv. Prof. Paper* 1313, R1-R17, 1983.
- White, R. M. and L. T. Long (1989). Evaluation of Hypotheses for the Cause of 1886 Charleston Earthquake, NUREG/CR-5269, 459 pp.
- Zoback, M. L., S. P. Nishenko, R. M. Richardson, H. S. Hasegawa and M. D. Zoback (1987). Mid-plate stress, deformation and seismicity, in The Geology of North America, Vol. M: The Western North Atlantic Region, P. R. Vogt, and B. E. Tucholke, (Editors), *Geol. Soc. Am.*, 297-312.

DEPARTMENT OF GEOLOGICAL SCIENCES
UNIVERSITY OF SOUTH CAROLINA
COLUMBIA SC 29201

Manuscript received 28 May 1991

generally
W but dip
and small
oriented
is oriented
are reverse

the others
Segrega-
oriented
or vertical
ing thrust
ing are in
faults in
classified as

vents that
dips and
suggests
0 m and 1
rmed with
lips. From
defines the
FZ.

reviewer for
dem for the
es Research

and M. C.
tectonics of
II, (Editors),

southeastern
Earthquake,

Stereograms,

ectonics and

n Appalachi-

to solve for
9 pp.

Determining
Geol. Surv.

when using

of 1886: A